Available online at www.sciencedirect.com

SciVerse ScienceDirect

Ceramics International 39 (2013) 2835–2843

CERAMICS INTERNATIONAL

www.elsevier.com/locate/ceramint

Alumina coatings on carbon bonded alumina nozzles for active filtration of steel melts

Christos G. Aneziris*, Steffen Dudczig*, Jana Hubálková, Marcus Emmel, Gert Schmidt

Institute of Ceramic, Glass and Construction Materials, Technical University of Freiberg, Germany

Received 12 July 2012; received in revised form 6 September 2012; accepted 15 September 2012
Available online 28 September 2012

Abstract

Slip casted, carbon bonded nozzles with and without alumina based active coatings have been simultaneously tested in a novel casting simulator according to their clogging behavior against endogenous as well as exogenous non-metallic inclusions. Computer tomography images as well as SEM micrographs support the investigation of the clogging areas. The nozzle with the alumina active coating leads to increased clogging phenomena based on endogenous and exogenous inclusions as well as steel clogged particles. Correlating the clogging to a type of improved "filtration efficiency", a higher filtration of steel melts is expected with the application of alumina active coatings on carbon bonded filters.

Keywords: D. Carbon; Filter; Clogging; Alumina

1. Introduction

Non-metallic inclusions in metal decrease dramatically the mechanical properties of castings [1], therefore ceramic filters in different macro-structure geometries [2–5] are successfully applied since several decades to remove non-metallic inclusions from ferrous and non-ferrous melts [6]. Besides the filter geometry, the ceramic material has a significant influence on the filtration efficiency particularly with regard to the active filtration process.

In the past Uemura et al. [5], Janke and Raiber [3], Morales et al. [7] and Hammerschmid and Janke [8] give an overview of the filtration mechanisms, filtration efficiencies, filter materials and filter structures for steel melts. According to Uemura et al. entrapment of the solid non-metallic inclusions by ceramic filters takes place in three steps: (a) the solid inclusions are transported from the bulk melt to the filter surface, (b) the inclusions are attached to the surface of the filter and (c) the inclusions undergo solid state sintering with the filter medium.

In order to eliminate the influence of the filter geometry, the filtration efficiency of the ceramic materials can be investigated in terms of clogging phenomena, whereby the pronounced clogging implicates high filtration efficiency. Clogging, an unrequested phenomenon in continuous casting nozzles, is the build-up of material in the flow passage between the tundish and the mold. Rackers and Thomas present four general types of clogging, each from a different origin.[9] Tuttle et al. [10] have studied clogging phenomena of refractory model nozzles based on carbon bonded alumina, calcium zirconate, calcium titanate and mixtures of the two oxide materials.

Based on the theoretical fundamentals of Janiszewski and Kudlinski [11], the application of active oxide coatings with the same chemistry as the chemistry of the inclusions in the melt is one very promising approach in order to collect more efficient liquid—as well as solid-non-metallic inclusions. In this study, two carbon bonded alumina nozzles – one with an active alumina coating and one without – will be simultaneously tested in a special steel casting simulator according to their clogging behavior against exogenous incorporated solid non-metallic inclusions.

2. Experimental

The functionality of the newly developed active carbon bonded filters [12] was evaluated in a new metal-casting

*Corresponding authors.
E-mail address: aneziris@ikgb.tu-freiberg.de (C.G. Aneziris).

0272-8842/$ - see front matter © 2012 Elsevier Ltd and Techna Group S.r.l. All rights reserved.
http://dx.doi.org/10.1016/j.ceramint.2012.09.055

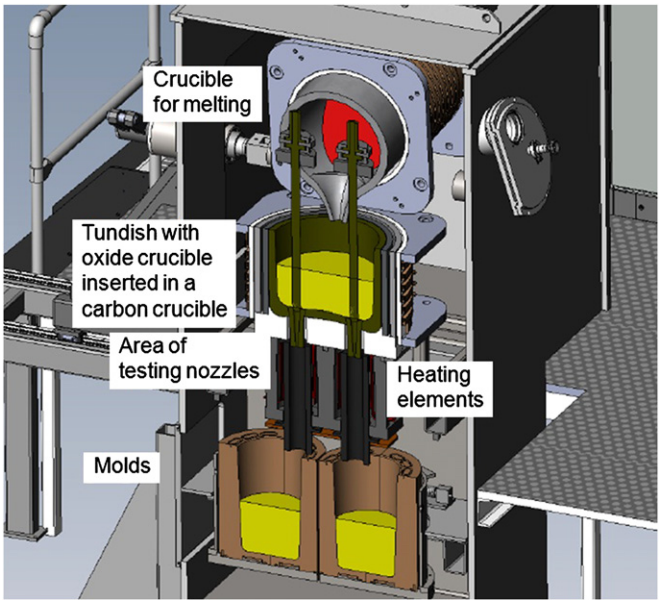

Fig. 1. Steel casting simulator.

simulator (Systec, Karlstadt, Germany) located at the Institute of Ceramic, Glass and Construction Materials in Freiberg. The system (Fig. 1) consists of a separated inductive-heated melting unit (150 kVA) and a tundish unit (inductive-heated 100 kVA) with three nozzles in the basement (two for tests and one for security reason) and a stopper rod system for controlling the melt flow. The melting crucible is based on zirconia/mullite (Colisit, Großalmerode, Germany) and the tundish unit consists of a carbon crucible in which an oxide crucible made from an in situ spinel forming/alumina-spinel castable is fitted in.

Commercial available steel DIN EN 42CrMo4 (Mat. no. 1.7225, AISI 4142) in cylindrical shape (72.5 kg) is placed in the melting crucible, heated up to 1650 °C in 90 min under inert atmosphere. The oxygen content and the temperature of the steel melt are measured with an oxygen/temperature-finger sensor-system CELOX (Heraeus Electro-Nite, Houthalen, Belgium). After melting, the steel melt is poured into the tundish unit, which is in advance preheated to prevent major heat loss of the melt and reduce also the thermal shock attack. A short time after pouring (ca. 30 s), the stoppers rods are lifted and the melt flows through the two test nozzles into the cooled copper molds. The test zone with the test nozzles (Fig. 2) is preheated by heating elements up to 1600 °C to prevent freezing of the liquid metal and to adjust a constant testing temperature in the nozzle area.

In Table 1 the composition of the slip casted carbon bonded nozzles as well as the slurry for the Al_2O_3-active coating on the carbon bonded alumina test nozzles are listed. The raw materials used for the preparation of the carbon bonded and the active carbon compositions were calcined alumina (99.80 wt% Al_2O_3, ≤ 0.10 wt Na_2O) with a $d_{90} \leq 3.0$ μm (Martinswerk, Bergheim, Germany), calcined alumina CL370 with a d_{50} 2.5 μm and a $d_{90} \leq 9.0$ μm (Almatis, Ludwigshafen, Germany), modified coal tar pitch powder

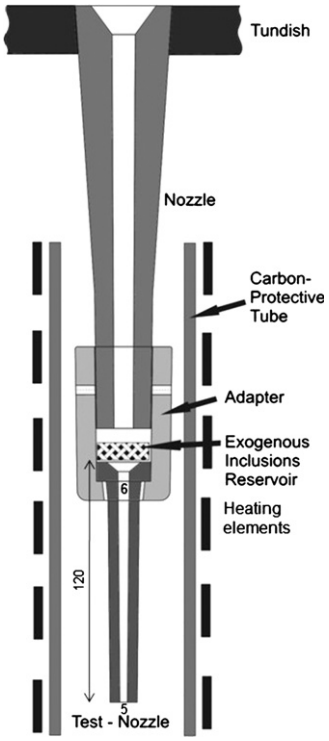

Fig. 2. Configuration of the testing nozzle area, test nozzle based on carbon bonded compositions with or without active alumina coating, adapter and nozzle above the testing nozzle based on spinel/alumina composition SP1 (see Table 3).

0–400 μm Carbores® P (Rütgers, Castrop Rauxel, Germany) used as binder as well as a carbon source, fine natural graphite grade AF 96/97 (99.8 wt% < 40 μm) with 96.7 wt% carbon content (Graphit Kropfmühl, Hauzenberg, Germany) and carbon black powder with a primary particle size of 200–500 nm (Lehmann & Voss & Co., Hamburg, Germany). The slurry was prepared in a ball mill by stepwise addition of above mentioned powders to the suspension of deionised water and following additives Lignisulfonate T11B (Otto Dille, Norderstedt, Germany), Castament VP 95L (BASF, Ludwigshafen, Germany) and Contraspum K 1012 (Zschimmer & Schwarz, Lahnstein, Germany). The carbon bonded test nozzles were slip casted in gypsum molds (5 mm thickness in approximately 5 min).

After slip-casting and drying at 120 °C for 24 h, the test-nozzles are fired at 800 °C in coke grit in order to inhibit the oxidation. Additionally some carbon bonded nozzles are coated with an alumina slurry (active coating, Table 1) by slip casting. The porous carbon bonded nozzle removes the water from the alumina slurry, i.e. it itself works like a gypsum mold. The alumina slurry was prepared in a ball mill by stepwise addition of alumina powders to the suspension of deionized water and following additives Lignisulfonate T11B (Otto Dille, Norderstedt, Germany), Dolapix PC75 (Zschimmer & Schwarz, Lahnstein, Germany), Polypropylenglycol PPG400 (Merck, Darmstadt, Germany) and Contraspum K 1012 (Zschimmer & Schwarz, Lahnstein, Germany). After coating and drying, the coated carbon bonded alumina nozzles were

fired at 1400 °C for 2 h in coke grit. In order to guarantee the same inner diameter of all test nozzles of 5 mm (tolerance range of 50 μm), gypsum molds with different geometries for the test nozzles with and without coating regarding the coating thickness and firing shrinkage were used.

On the top of the test-nozzle a 10 ppi (pores per inch) alumina carbon bonded filter is placed (composition listed in Table 1). In case of the filter an impregnation as well as a spray-coating slurry are used according to Emmel and Aneziris [13]. After coking at 800 °C, the filter was spray-coated with an alumina/spinel/mullite slurry (composition listed in Table 2) and dried at 120 °C for 24 h. The only dried spray-coated filter contributes as a source of exogenous solid non-metallic inclusions (approximately 3.15 gr. exogenous inclusions) during the steel casting.

The adapter system, the stoppers and the nozzles are made from an in situ spinel forming/alumina-spinel castable fired at 1600 °C. It is a self-flowing castable with the size distribution modulus of 0.28 based on the Dinger and Funk particle-packing equation [14].

The alumina carbon bonded slurry as well as the alumina slurry for the active coating of the slip casted test nozzles were characterized using a rheometer (RS 150, Haake, Vreden, Germany) with a coaxial cylindrical measurement system (DIN 53019) and Z40 DIN system. The viscosity was determined in dependence of the shear rate and the yield stress was measured. The measurement of the viscosity starts after a relaxing time of 20 s when the shear rate increases in 300 s to 1000 1/s. After a holding time of 60 s at 1000 1/s, it decreases within 300 s to zero.

The test nozzles before and after pouring as well as the adapter with the filter and nozzle after pouring were analyzed with the aid of a microfocus X-ray computed tomograph CT-ALPHA (ProCon X-Ray, Garbsen, Germany). The CT is equipped with a 160 kV X-ray source and a detector C7942SK-05 (Hamamatsu, Hamamatsu, Japan) with 2024 × 2024 active pixels. For the visualization of CT-images the software VGStudio Max 2.1 (Volume Graphics GmbH, Heidelberg, Germany) was used.

The microstructural phase evaluation of as coked surfaces as well as of fracture surfaces after firing and after pouring were carried out by means of scanning electron microscope ESEM (Philips, Germany) and SEM XL30 (Philips, Germany) with the implementation of electron backscatter diffraction analyses EBSD system TSL (Edax/Ametek, Wiesbaden, Germany) in combination with energy dispersive spectrometer (EDS).

The surface characterization of the test nozzles was supported by mercury porosimetry measurements with the aid of porosimeter Pascal L 140 (Thermo Electron Coop., Hofheim, Porotec). The chemical analysis of the steel before melting and after casting was measured with

Table 1
Compositions of Al_2O_3-C spraying and impregnating slurries, and Al_2O_3-slip casting slurry.

Slurry types	**Filter recipe** (wt%)	**Al_2O_3-C nozzle** (wt%)	**Al_2O_3 active coating on Al_2O_3-C nozzle** (wt%)
Impregnation-slurry	82 solids		
Spray-coating	70 solids		
Slurry for slip casting		60 solids	70 solids
Solids			
Al_2O_3 Martoxid MR 70	66	66	
Al_2O_3 CL370	–	–	100
Carbores® P	20	20	
Graphite AF 96/97	6.3	6.3	
Carbon black MTN-991	7.7	7.7	
Ligninsulfonate[a] T11B	1.5	1.5	1.5
Castament VP 95L[a]	0.3	0.3	
Contraspum K 1012[a]	0.1	0.1	0.1
Dolapix PC75[a]			0.5
Polypropylenglycol 400[a]			0.8

[a]Related to the solids.

Table 2
Slurry composition of exogenous inclusions based on alumina, mullite and spinel.

Raw materials	**Composition of the slurry** (wt%)	**Distribution** (μm)	D_{50} (μm)	D_{90} (μm)
Solids	70.0			
Al_2O_3 T 60/64 (Almatis, Ludwigshafen, Germany)	37.6	0–100	31.1	99
Mullite Fused (Treibacher, Villach, Austria)	34.0			
Spinel AR 78 (Almatis, Ludwigshafen, Germany)	28.4	0–90	20	–

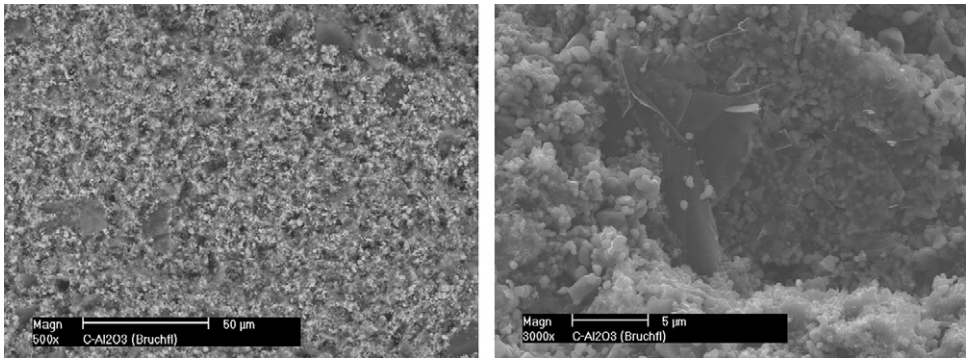

Fig. 3. Cross section of carbon bonded nozzle, fine alumina grains and graphite flakes embedded in carbon bonded matrix.

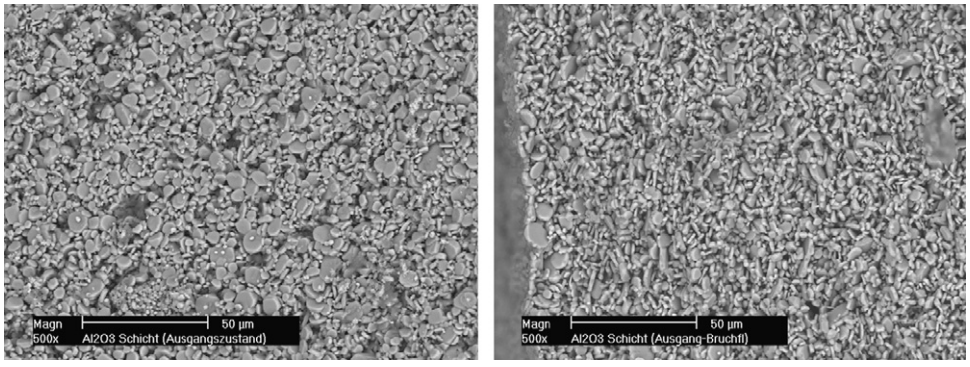

Fig. 4. Surface (left) and cross section (right) of alumina active coating on carbon bonded alumina nozzle after firing at 1400 °C.

the aid of spark source spectrography MAXx (Spectro Analytical Instruments/Ametek, Wiesbaden, Germany).

3. Results and discussion

The Al_2O_3-C-slurry described in Table 1 for manufacturing the carbon bonded nozzles with and without an active coating shows a shear thinning behavior with a dynamic viscosity of approx. 80 mPa s at a shear rate of 800 s^{-1}. The Al_2O_3-slurry for the alumina active coating presents less than 40 mPa s at a shear rate of 800 s^{-1}. In spite the fact that this slurry shows a shear thickening behavior, it is possible to prepare fine, stabilized slurries (no sedimentation of solids after 24 h) due to the low viscosity under shearing conditions. The stabilized slurries were used for the slip casting of the test nozzles with small deviation of the inner diameters at the different sections after firing. Based on CT-images the radius at the down end of both nozzle types is lying in the range of 5.05 ± 0.05 mm after firing.

In Fig. 3 the microstructure of the carbon bonded alumina material is demonstrated. Fine alumina grains and graphite flakes are embedded in a carbon bonded matrix generated due to firing of the binder Carbores P. The residual carbon after firing Carbores P at 800 °C reaches values in the range of approximately 85% and it presents a graphitic-like structure with a high crystallinity as it is described by Aneziris et al. [15] and Emmel and Aneziris [13] after firing at 1400 °C.

In Fig. 4 the alumina layer deposited on the carbon bonded alumina nozzle after firing at 1400 °C in reducing atmosphere is presented. This layer does not have any chemical bonding with the carbon bonded alumina substrate, and due to mechanical interlocking it remains on the carbon bonded alumina nozzle. In Fig. 5 the pore size distribution of the carbon bonded alumina materials fired at 800 °C and 1400 °C respectively are plotted. The total porosity lies at 44 vol% for the carbon bonded material fired at 800 °C and is decreased to 39.7 vol% for the material fired at 1400 °C. In spite the fact that the total porosity reaches lower values by firing at higher temperatures, the average pore diameter lies for both firing temperatures in the range of 190 nm. The alumina active coating achieves lower values of the total porosity in the range of 33.3 vol%, but in this case the average pore diameter lies at 530 nm. Based on the pores size distribution in Fig. 6 also some bigger pores greater than 10 µm are identified for the alumina active coating.

The oxygen amount of the steel-melt in the melting crucible at 1650 °C just before pouring into the tundish was 55 ppm. In Table 3 the compositions of the steel before melting and after casting are listed. The Al-contents in both steel ingots (of the nozzle with and without the alumina active coating) are decreased, an indication of possible generation of endogenous alumina inclusions.

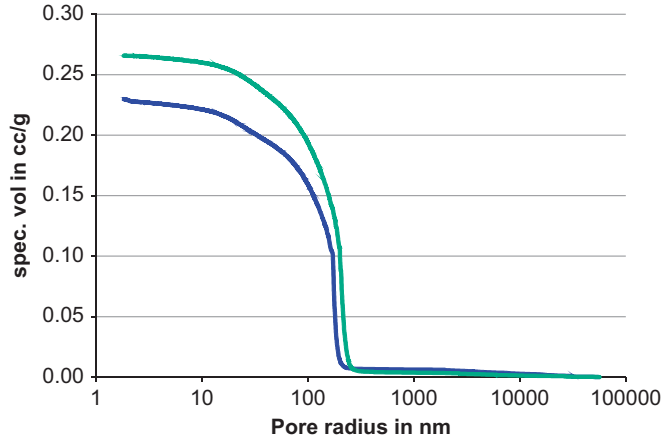

Fig. 5. Pore size distribution of carbon bonded nozzles fired at 800 °C and 1400 °C without an alumina coating.

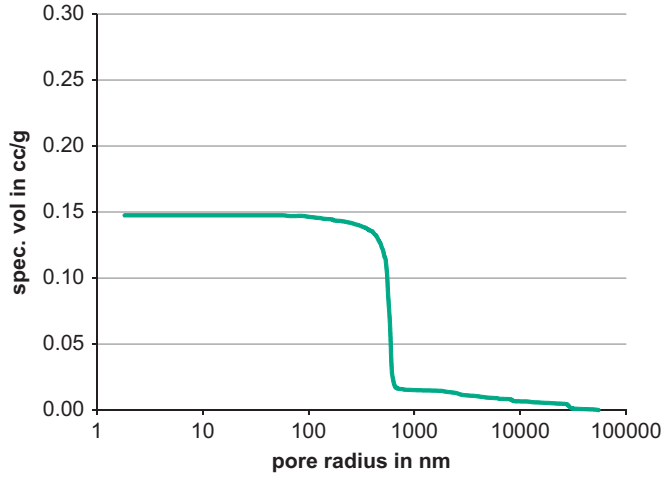

Fig. 6. Pore size distribution of alumina active coating after firing at 1400 °C.

In Fig. 7 the changes of the flow rates of the two nozzle types as a function of time are demonstrated. After 130 s approximately 36.54 ± 0.1 kg steel passed through the reference carbon bonded nozzle and 35.49 ± 0.1 kg through the carbon bonded nozzle with the alumina active coating (in spite the fact, that both nozzles had approximately the same starting inner geometry). A second trial with the same arrangement showed a small deviation of 200 g casted more through the not functionalized nozzle. Both trials presented a similar behavior of the flow. During the first stage of the flow (approx. the first 60 s) a thermal balance as well as balanced flow conditions are established. Concerning the balanced flow conditions, a vortex generation in the tundish above the nozzles after lifting the stopper is observed through a refractory glass port. It is assumed, that this vortex contributes to lower flow rates in the nozzles. After the first stage, the flow rates are increasing, whereby a higher increase is registered in case of the reference carbon bonded nozzle (second stage).

Table 3
Chemical composition of the steel (main elements) before melting and after casting (average of three measurements).

Element	Content (wt%)		
	Before melting	After casting	
		With alumina-coating	Without coating
Fe	96.65	96.93	96.95
Cr	1.03	1.09	1.09
C	0.43	0.34	0.34
Mn	0.78	0.66	0.66
Cu	0.29	0.28	0.29
Al	**0.022**	**0.006**	**0.005**
Si	0.26	0.26	0.24
Ni	0.22	0.16	0.16
Mo	0.19	0.18	0.18
S	0.041	0.015	0.018
Sn	0.016	0.015	0.014
P	0.016	< 0.001	< 0.001
N	0.008	0.006	0.006
V	0.006	0.006	0.006
Ti	0.002	< 0.001	< 0.001

As a function of time, the flow rates of both nozzles are decreased due to less steel melt in the tundish (lower ferrostatic pressure), third stage. The lower total amount of poured steel melt as well as the lower flow rates in case of the nozzle with the alumina active coating are attributed to clogging phenomena.

In Fig. 8 a cross section of the adapter with the carbon bonded nozzle containing alumina active coating is presented. It is evident that a clogging preferred occurs in the down area of the carbon bonded nozzle (20 mm from the down end). Due to the resolution of the CT and the lower thickness of the clogging layer of the reference carbon bonded alumina nozzle, no clogging could be identified for the reference nozzle with the aid of CT. In Fig. 9 the changes in the thickness of the alumina coating due to the clogging is registered. The thickness of the alumina active coating before casting was 350 ± 20 μm at the voxel size of 23 μm. The highest absolute clogging values are registered just before the end of the nozzle lying in the range of 170 ± 60 μm. In Fig. 10 the cross-section CT-images of the clogged carbon bonded nozzle with alumina active coating 1.5 mm from the end of the nozzle is presented. Non-metallic inclusions, clogged steel particles as well as non-metallic inclusions on the top of the embedded steel particles are registered. In accordance with Rackers and Thomas [9] this clogging type correlates to steel qualities with more than 0.1% C.

In Fig. 11 the clogging area approx. 8 mm from the down end of the carbon bonded nozzle with the active alumina coating is presented. Two main clogging areas are identified, (a) a "denser clogging area" in the range of 35 μm, which is mostly fixed at the alumina active coating, and (b) a "coral-like clogging area" in the range of 50 μm as also described by Tuttle et al. [10]. The "denser clogging

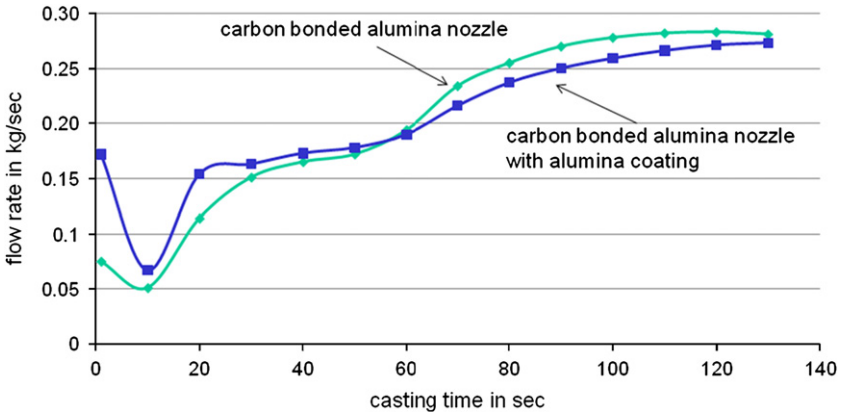

Fig. 7. Flow rates as a function of time of the carbon bonded nozzle with alumina coating and the reference carbon bonded alumina without coating.

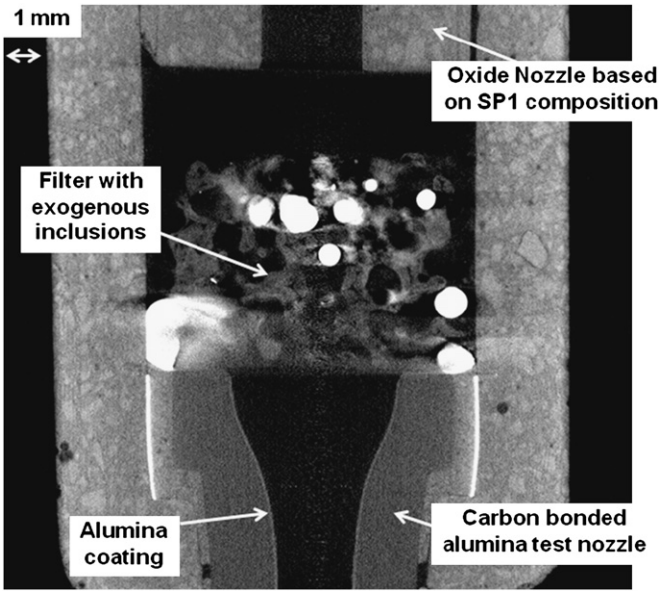

Fig. 8. CT-image of the adapter with carbon bonded nozzle with alumina active coating after casting, on the top of the nozzle a carbon bonded filter with exogenous inclusions.

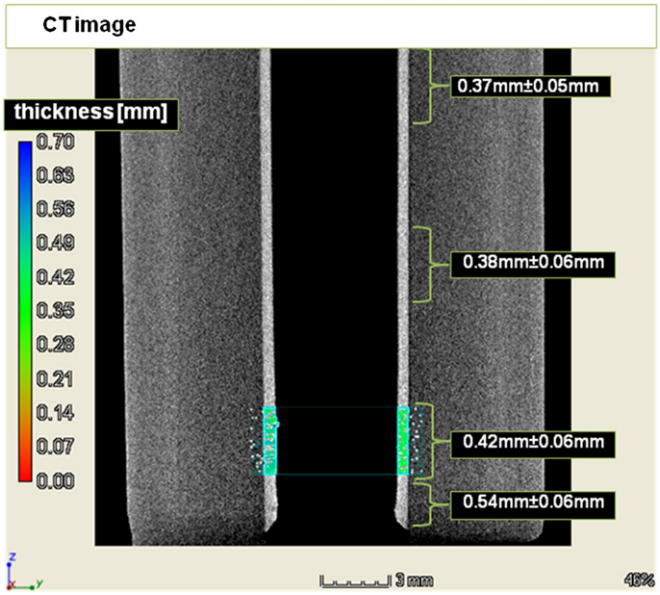

Fig. 9. Down part (approx. 20.7 mm) of the carbon bonded nozzle with alumina coating and, thickness variation due to clogging, 23 μm voxel resolution.

area'' consists of steel clogged small and bigger particles, especially the bigger ones in the range of 5–15 μm. These bigger steel particles are surrounded by smaller alumina particles in the range of 100–300 nm as well as bigger alumina particles between 1 and 5 μm. Based on the grain size distribution of the exogenous inclusions that have been inserted in the melt flow with the aid of the filter above the carbon bonded nozzle, the bigger alumina particles are defined as exogenous inclusions. The smaller alumina particles in the magnitude below 500 nm are identified as endogenous inclusions similar to the observations of Wasai et al. [2] in their contribution. Besides the alumina based non-metallic inclusions also spinel exogenous inclusions in the range of 1 to up to 8 μm are registered (Fig. 12). The ''denser clogging area'' consists of a dense network of endogenous and exogenous non-metallic inclusions as well as smaller and especially bigger steel clogged particles. In Fig. 13 the clogging area approx. 20 mm from the down end is presented. In this case, the magnitude of the denser clogging area is lower in comparison to the clogging microstructure of Fig. 11 (8 mm from the down end). On the other hand a bigger ''coral-like clogging area'' in the range of 80 μm is registered. According to the magnification of Fig. 13 exogenous alumina inclusions are captured in the ''coral-like clogging area'' based mainly on endogenous inclusions (in the range of 100–300 nm), Fig. 14. Further, sintering effects between exogenous and endogenous inclusions are registered as well as steel clogged particles surrounded by exogenous and endogenous inclusions, Fig. 14.

The clogging phenomena of the reference nozzle without an alumina active coating are also concentrated in the down part, approximately 20 mm from the down end, whereby again the highest clogging area is identified in the range of 1–5 mm from the down end. In this case, the

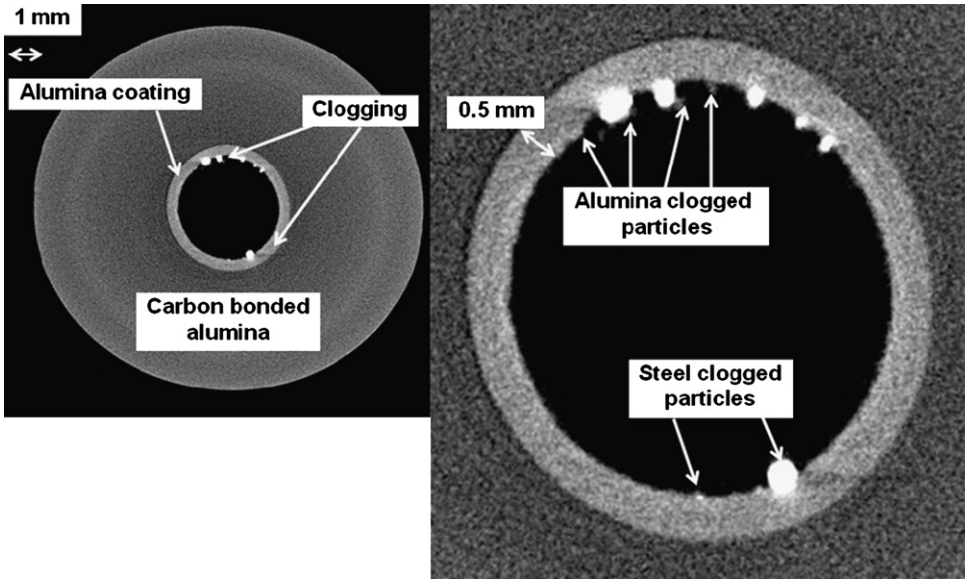

Fig. 10. CT-image of the clogged carbon bonded nozzle with alumina coating 1.5 mm from the end of the nozzle.

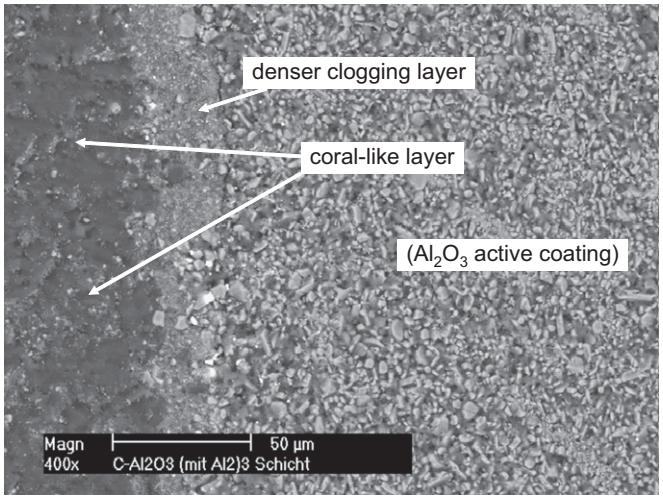

Fig. 11. Clogging area approx. 8 mm from the down end, two main clogging areas (a) denser clogging area in the range of 35 µm and (b) coral-like clogging area in the range of 60–80 µm.

''denser clogging area'' as well as the ''coral-like clogging area'' present lower thicknesses in comparison to the nozzle with the alumina active coating lying in the range of 30–20 µm respectively. The thin clogging layer could not be identified using CT-images because of the voxel size of 23 µm (too low resolution for the detection of the layers in the range of 20–30 µm). Nevertheless, clogged non-metallic inclusions, steel particles and spinel as well as alumina non-metallic inclusions were identified using BSE and EDS-mapping and confirmed with the aid of EBSD. By means of EDS no diffusion of iron and/or manganese was registered, i.e. both, iron and manganese, are incorporated in the spinel cell lattice.

In contradiction to these results, the spinel particle in the carbon nozzle with the alumina active coating (Fig. 12) in contact with the steel clogged particle presents much higher amounts of iron and manganese at its grain boundaries. In case of the non-metallic inclusions a very high amount of iron and aluminum was registered, and the formation of $FeAl_2O_4$ was identified with the aid of EDS analysis. Kapilashrami and Seetharaman [16] have found similar results (formation of a product layer based on $FeAl_2O_4$ of approximately 80 µm between the alumina and the iron) by studying the wetting characteristics of oxygen-containing iron melts on alumina.

Comparing the clogging of the two nozzles according to the thickness of the ''denser clogging area'' in a distance of 1–8 mm from the down end, the nozzle with the alumina active coating presents an average clogging thickness of approximately 90 ± 20 µm, whereby the nozzle without the alumina coating an average clogging thickness of 20 ± 10 µm. Correlating these values to a type of ''filtration efficiency'' in means of more particles (endogenous and exogenous non-metallic inclusions as well as clogged steel particles with or without additional non-metallic inclusions on their surface) to be deposited on the ceramic collector surface (nozzle or filter), there is a first indication that at least a double filtration efficiency is expected in case of coated carbon bonded filters. This issue has to be verified with the mechanical properties of the steel ingots as well as transferred to real filter geometries.

According to Uemura et al. the sintering neck between two alumina based non-metallic inclusions in the range of 2.5 µm is growing 0.1 µm in less than 0.03 s. Taking into account that the shear stress working on the sintered part of inclusions due to the drag force achieves values less than 1×10^8 Pa and the strength of alumina is about 3×10^8 Pa,

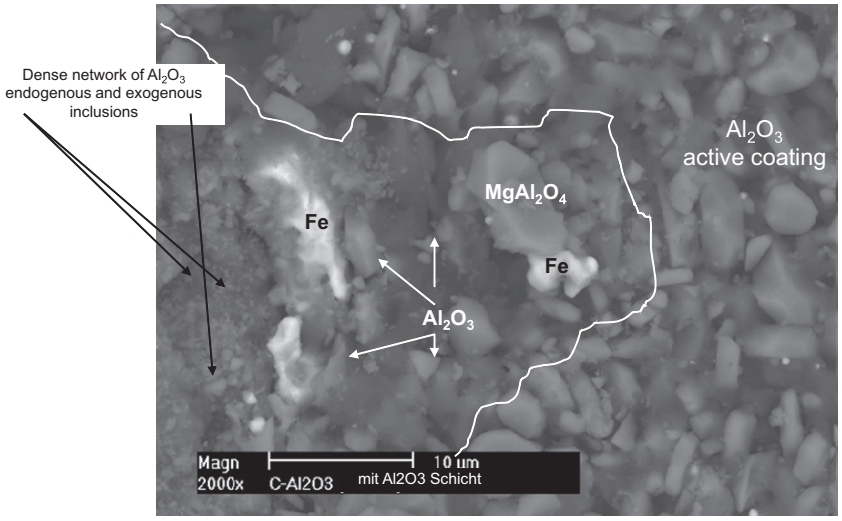

Fig. 12. Clogging area approx. 8 mm from the down end, alumina and spinel inclusions with embedded iron particles.

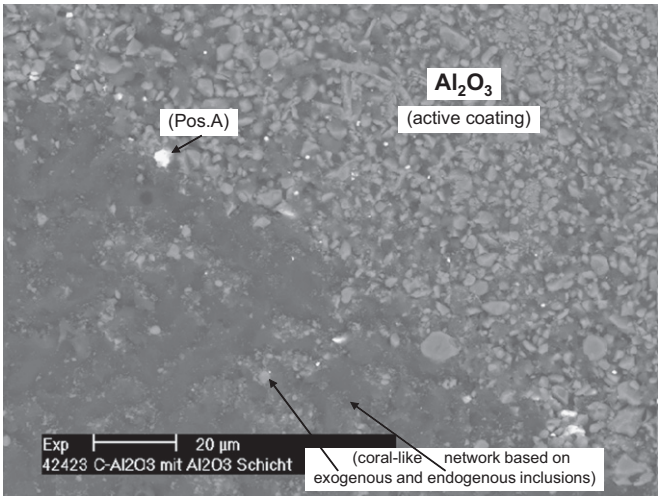

Fig. 13. Clogging area approx. 20 mm from the down end.

the inclusions that are kept at the ceramic surface (in our case the nozzle, in real application the filter surface) for short time, they also stick to the surface. Based on the SEM-micrographs of Figs. 12 and 14 sintering effects are observed between alumina endogenous and/or exogenous inclusions as well as between endogenous and exogenous alumina inclusions with exogenous spinel inclusions. Further, in case of the nozzles with the alumina active coating a higher amount of clogged steel as well as bigger steel clogged particles can be observed. The steel clogged particles can contribute in addition as collectors for fine and coarse alumina inclusions due to a product formation layer based of hercynite ($FeAl_2O_4$), which lowers the wetting angle between alumina and iron. According to Kapilashrami and Seetharaman mullite could react with iron in order to form product layers based on hercynite and fayalite.

The higher clogging of the carbon bonded nozzle with the alumina active coating results also to less passed steel melt as a function of time (as it has been registered in Fig. 7). Thereby, it is assumed that not only the change of the thickness of the inner diameter of the nozzle, but also the generated roughness is significant for the different flow behavior.

4. Conclusions

Carbon bonded nozzles with and without alumina active coatings have been simultaneously tested in a novel steel casting simulator according to their clogging performance against endogenous as well as exogenous non-metallic inclusions. A ''denser'' as well as a ''coral-like clogging area'' have been identified in both cases, whereby higher clogging has been registered in the nozzles with the active alumina coating. The ''dense clogging layer'' consisted of endogenous and exogenous non-metallic inclusions as well as steel clogged particles with inclusions on their surface. Some of the non-metallic inclusions at the steel clogged particles have reacted with the iron and hercynite was formed. Endogenous and exogenous alumina inclusions as well as spinel exogenous inclusions sinter together and contribute to the formation of the two clogging areas.

The higher clogging of the carbon bonded alumina nozzle with the active alumina coating led also to less pass of the steel melt through the nozzle. The lower flow is attributed to the clogging layer, especially to its roughness, the smaller inner diameter of the nozzle and the new chemistry of the layer in means of possible local Marangoni flow phenomena.

Correlating these clogging values to a type of ''filtration efficiency'' in means of more particles to be deposited on the ceramic collector surface (nozzle or filter), there is a first indication that at least a higher filtration efficiency is expected in case that carbon bonded filters are coated with an alumina active coating. The interactions of the above mentioned issues on clogging as well as the possible higher

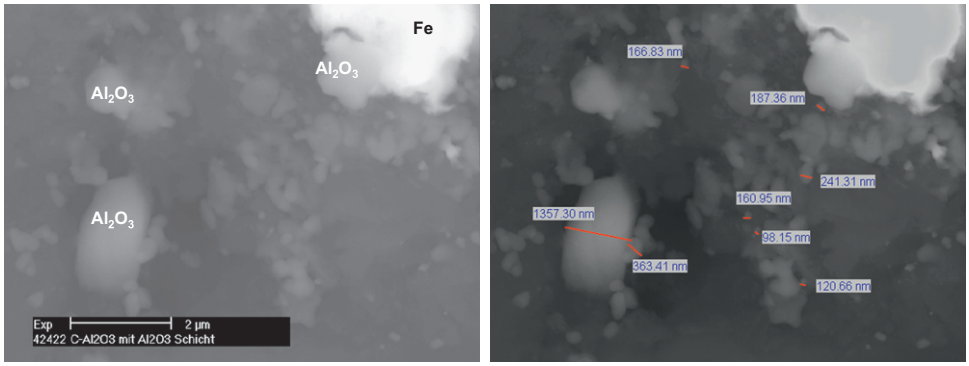

Fig. 14. Magnification of Fig. 13, clogging area approx. 20 mm from the down end, exogenous alumina inclusions captured in the "coral-like clogging area" based on endogenous inclusions in the range of 100–300 nm, sintering effects between exogenous and endogenous inclusions, and steel clogged particles surrounded by exogenous and endogenous inclusions.

filtration efficiency with the aid of active and/or reactive coatings will be investigated in the future in more detail.

Acknowledgments

This work was financially supported by the German Research Foundation (DFG) in frame of the Collaborative Research Center 920. The authors would like to thank Mr. R. Fricke for the technical support of the tests in the steel casting simulator and Mr. J. Aurich for the spark source spectrography analysis.

References

[1] L. Zhang, B.G. Thomas, Inclusions in Continous Casting of Steel, in: Proceedings of the XXIV National Steelmaking Symposium, Morelia, Mich, Mexico, 26–28, November 2003, pp. 138–183.

[2] (a) K. Wasai, K. Mukai, A. Miyanaga, Observation of inclusion in aluminum deoxidized iron, ISIJ International 42 (2002) 459–466;
(b) C.G. Aneziris, A. Ansorge, H. Jaunich, New approaches of carbon bonded foam filters for filtration of large castings, Ceri Forum International, Special Refractories for Clean Steel Technology 85 (2008) E100–E103.

[3] D. Janke, K. Raiber, Grundlegende Untersuchungen zur Optimierung der Filtration von Stahlschmelzen, Technische Forschung Stahl, Luxembourg Europäische Kommission, 1996, ISBN:92-827-6458-3.

[4] D.M. Essock, H. Jaunich, C.G. Aneziris, J. Hubalkova, Novel foamless ceramic filters for advanced metal casting, in: Proceedings of the UNITECR '05, 2005, pp. 667–669.

[5] K. Uemura, M. Takahashi, S. Koyama, M. Nitta, Filtration mechanism of non-metallic inclusions in steel by ceramic loop filter, ISIJ International 32 (1992) 150–156.

[6] O. Davila-Maldonado, A. Adams, L. Oliveira, B. Alquist, R.D. Morales, Simulation of fluid and inclusions dynamics during filtration operations of ductile iron melts using foam filters, Metallurgical and Materials Transactions B 39 (2008) 818–839.

[7] R.D. Morales, O. Davila-Maldonado, A. Adams, L. Oliveira, B. Alquist, Computer and fluid flow modeling of filtration mechanisms in foam filters, AFS Transactions (2008) 715–731.

[8] P. Hammerschmid, D. Janke, Kenntnisstand zur Abscheidung von Einschlüssen beim Filtrieren von Stahlschmelzen, Stahl und Eisen 108 (1988) 211–219.

[9] K.G. Rackers, B.G. Thomas, Clogging in continuous casting, in: Proceedings of the 78th Steelmaking Conference, Nashville, Iron and Steel Society, vol. 78, 1995, pp. 723–734.

[10] R.B. Tuttle, J.D. Smith, K.D. Peaslee, Casting simulation of calcium titanate and calcium zirconate nozzles for continuous casting of aluminum-killed steels, Metallurgical and Materials Transactions B 38 (2007) 101–108.

[11] K. Janiszewski, Z. Kudlinski, Removal of liquid non-metallic inclusion from molten steel using the method filtration, Metal (2006) 1–9.

[12] C.G. Aneziris, M. Emmel, A. Stolle, Multifunctional carbon bonded filters for metal melt filtration, review, in: Proceedings of the 36th International Conference and on Advanced Ceramics and Composites, American Ceramic Society, January 2012.

[13] M. Emmel, C.G. Aneziris, K.D. Peaslee, Development of novel carbon bonded filter compositions for steel filtration, Ceramic International 38 (2012) 5165–5173.

[14] J.E. Funk, D.R. Dinger, Particle size control for high-solids castable refractories, American Ceramic Society Bulletin 73 (1994) 66–69.

[15] C.G. Aneziris, F. Homola, D. Borzov, Materials and process development of advanced refractories for innovative metal processing, Advanced Material Engineering 6 (2004) 470–562.

[16] E. Kapilashrami, S. Seetharaman, Wetting characteristics of oxygen-containing iron melts on refractory oxides, Journal of Materials Science 40 (2005) 2371–2375.